Applied Physics Letters

Stabilization and control of topological magnetic solitons via magnetic nanopatterning of exchange bias systems

Cite as: Appl. Phys. Lett. **113**, 162401 (2018); https://doi.org/10.1063/1.5047222
Submitted: 05 July 2018 . Accepted: 19 August 2018 . Published Online: 15 October 2018

Edoardo Albisetti, Annalisa Calò, Martin Spieser, Armin W. Knoll, Elisa Riedo, and Daniela Petti

COLLECTIONS

This paper was selected as Featured

View Online Export Citation CrossMark

ARTICLES YOU MAY BE INTERESTED IN

Study of spin-orbit torque induced magnetization switching in synthetic antiferromagnet with ultrathin Ta spacer layer
Applied Physics Letters **113**, 162402 (2018); https://doi.org/10.1063/1.5045850

Perspective: Magnetic skyrmions–Overview of recent progress in an active research field
Journal of Applied Physics **124**, 240901 (2018); https://doi.org/10.1063/1.5048972

The design and verification of MuMax3
AIP Advances **4**, 107133 (2014); https://doi.org/10.1063/1.4899186

Lock-in Amplifiers up to 600 MHz
Watch

AIP Publishing

© 2018 Author(s).

Stabilization and control of topological magnetic solitons via magnetic nanopatterning of exchange bias systems

Edoardo Albisetti,[1,2,a)] Annalisa Calò,[1] Martin Spieser,[3] Armin W. Knoll,[4] Elisa Riedo,[1,5] and Daniela Petti[2]

[1]*Advanced Science Research Center, CUNY Graduate Center, 85 St. Nicholas Terrace, New York, New York 10031, USA*
[2]*Dipartimento di Fisica, Politecnico di Milano, 20133 Milano, Italy*
[3]*SwissLitho AG, 8805 Zürich, Switzerland*
[4]*IBM Research-Zurich, 8803 Rüschlikon, Switzerland*
[5]*Tandon School of Engineering, New York University (NYU), 6 MetroTech Center Brooklyn, New York, New York 11201, USA*

(Received 5 July 2018; accepted 19 August 2018; published online 15 October 2018)

Stabilizing and manipulating topological magnetic quasiparticles in thin films is of great interest for potential applications in data storage and information processing. Here, we present a strategy for stabilizing magnetic vortices and Bloch lines with controlled position, vorticity, and chirality in a continuous exchange bias system. By tailoring vectorially the unidirectional anisotropy of the system at the nanoscale, via thermally assisted magnetic scanning probe lithography, we show experimentally and via micromagnetic simulations the non-volatile creation of vortex-antivortex pairs. In addition, we demonstrate the deterministic stabilization of cross and circular Bloch lines within patterned Néel magnetic domain walls. This work enables the implementation of complex functionalities based on the control of tailored topological spin-textures in spintronic and magnonic nanodevices. *Published by AIP Publishing.* https://doi.org/10.1063/1.5047222

Topologically protected magnetic spin-textures, such as magnetic vortices, Bloch lines, and skyrmions, are increasingly attracting attention for their applications in a wide variety of fields, ranging from data storage and processing[1–5] to medicine.[6] For example, in racetrack memories,[7–9] the information is stored by means of magnetic quasiparticles which are controllably stabilized and manipulated via external stimuli within nanowire-based spintronic devices. The dynamic properties of vortices, i.e., their excitation, the core reversal, and their coupling,[10–14] have been extensively studied and are at the basis, for example, of magnetic vortex oscillators.[15–17] Furthermore, the spin-texture topology has a crucial role in the propagation of domain walls.[18,19] The interaction of vortices with spin-waves has been investigated,[20–22] and in particular, recently, the use of vortex cores as emitters of short-wavelength spin-waves was demonstrated.[23]

For all these applications, the development of methods for stabilizing and manipulating topological solitons is of capital importance. Among these methods, patterning ferromagnetic micro- and nano-structures such as disks or ellipses is widely employed, and it allows the stabilization of vortices (with topological winding number +1) by exploiting the shape anisotropy of the system, which favors the circulation of the magnetization, for removing magnetostatic charges at the disk edges.[24,25] The injection of a spin-polarized current in the nanocontact geometry is a well-established method for nucleating vortex-states in a continuous film through spin-transfer torque.[26] The controlled stabilization of antivortex ground states (with topological winding number −1), on the other hand, is more challenging and is usually achieved as a result of the stabilization of multiple vortices in a vortex-antivortex (V-A) array.[17,27–29]

Nevertheless, positioning and manipulating single topological spin-textures with deterministically controlled position, vorticity and chirality, and in a non-volatile way, is extremely challenging. In this work, we demonstrate a straightforward strategy for stabilizing and manipulating with nanoscale precision magnetic topological solitons, by reversibly patterning the unidirectional anisotropy of a continuous exchange bias system via thermally assisted magnetic scanning probe lithography (tam-SPL).[30–33] In particular, we show experimentally and with micromagnetic simulations the non-volatile stabilization and manipulation of vortices with tailored vorticity and chirality and the nucleation of single Bloch lines within patterned Néel domain walls. Furthermore, we show that Bloch lines stabilized within patterned arbitrarily shaped domain walls can be controllably displaced along the wall via static external fields.

The studied systems consist of $Ir_{22}Mn_{78}$ 7-10/$Co_{40}Fe_{40}B_{20}$ 5-20/Ru 2 (thicknesses in nm) multilayers grown via magnetron sputtering as reported in Ref. 30, featuring an exchange bias field ranging from 2.5 to 9 mT, depending on the antiferromagnetic and ferromagnetic film thicknesses. Tam-SPL was performed via NanoFrazor Explore (SwissLitho AG, Zurich), a commercial thermal scanning probe lithography system, using a cantilever design (see supplementary material note 1) that provides higher tip heater temperatures compared to the previous design[34] at temperatures higher than the silicon inversion temperature. For patterning, the thermal probe was swept on the sample surface in a raster-scan fashion and heated via joule effects by applying voltage pulses across the heater region of the cantilever. The heating time was 40 μs/pixel, with a 10 nm × 10 nm

[a)]Author to whom correspondence should be addressed: edoardo.albisetti@polimi.it

pixel size and a 100 μs/pixel time. For patterning regions with different exchange bias directions, the orientation of the external magnetic field during the localized field cooling was controlled by a rotatable permanent magnet which generated a uniform 600 Oe magnetic field directed within the plane of the sample. Micromagnetic simulations of the ground state of the exchange bias system were carried out by solving the Landau-Lifshitz-Gilbert equation, using the software MuMax3.[35] The total simulated volume had dimensions $5120 \times 5120 \times 5\,\text{nm}^3$ with a cell size of $5 \times 5 \times 5\,\text{nm}^3$ and a periodic boundary condition in the x-direction. For the CoFeB film, the saturation magnetization was $M_s = 1140\,\text{kA/m}$, and the exchange constant was $A_{ex} = 1.2 \times 10^{-11}$ J/m. The Gilbert damping parameter was set to $\alpha = 0.5$. The exchange bias field was modeled as an external magnetic field with different in-plane directions and strengths, as indicated.

In Fig. 1, we demonstrate the controlled nucleation of vortex-antivortex pairs in a CoFeB 5/IrMn 7/Ru 2 (dimensions in nm) exchange bias system. The patterned exchange bias field configuration [panels (a) and (d)], the Magnetic Force Microscopy (MFM) image [panels (b) and (e)], and the results of micromagnetic simulations [panels (c) and (f)] are presented. Blue arrows indicate the direction of the patterned exchange bias field, and black arrows the direction of the magnetization. In the micromagnetic simulation, the red and blue colors indicate the divergence of the magnetization, which is related to the experimental MFM contrast. In panels (a)–(c), we show that a vortex-antivortex pair is stabilized by patterning sequentially 4 triangular-shaped areas with unidirectional anisotropy oriented in a counterclockwise direction. Outside the patterned area, the unidirectional anisotropy is uniformly directed along $-x$. Such a non-uniform configuration

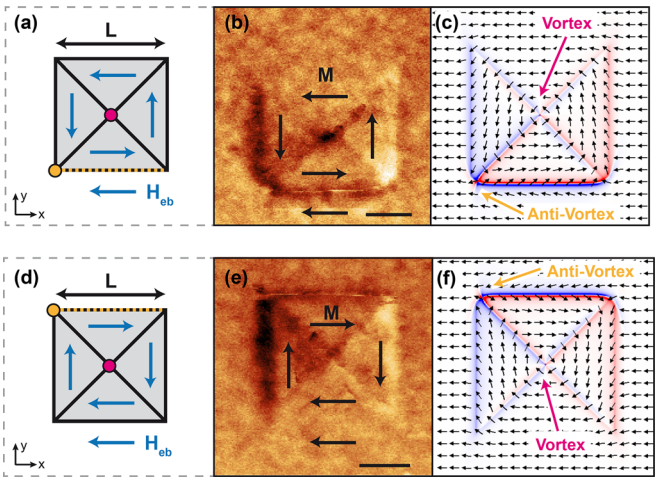

FIG. 1. Stabilization of vortex-antivortex pairs. (a) and (d) Schematics showing the configuration of the exchange bias patterned via tam-SPL in the IrMn/CoFeB system, for counterclockwise and clockwise chirality, respectively. The direction of the patterned exchange bias is indicated by the blue arrow for each area. L marks the lateral size of the pattern. The pink (orange) circles mark the position of the vortex core (antivortex) within the pattern. The orange dotted line marks the 180° Néel domain wall. (b) and (e) MFM images of the patterned structure for counterclockwise and clockwise orientations, respectively. The direction of the magnetization is indicated by the black arrows. The scale bar is 2 μm. (c) and (f) Corresponding simulated micromagnetic configuration showing the location of the vortex and antivortex. The black arrows indicate the direction of the spins, and the red/blue color marks div (**M**), which is related to the measured MFM contrast.

of the exchange bias field, which in turn stabilized a complex non-uniform magnetization configuration, generates a local potential minimum for the vortex core in the center of the patterned region [pink circle in panels (a) and (d)] and an antivortex core at the boundary of the patterned region (indicated with a yellow circle). The MFM image and micromagnetic simulation of the pattern at remanence confirm the stabilization of two 90° domain walls on the lateral sides of the square pattern and one 180° wall on the bottom side. It is worth noting that the 180° Néel wall, marked by a yellow dashed line in the sketch, constitutes equilibrium positions for the antivortex core, which can be displaced from its initial position via external fields, as it will be discussed in the following. We verified the stability of the patterned magnetic configuration over time by remeasuring the patterns after 8 months (see also Ref. 30). We remark that the process of field cooling and the exchange bias are also exploited for memory applications,[36] magnetic sensing[37] and local stray field design.[38] The properties of the vortex-antivortex pairs can be tailored by controlling the direction of the patterned exchange bias field with respect to the geometrical shape of the patterned area. In particular, as shown in panels (d)–(f), by changing the direction of the patterned exchange bias field, the chirality of the vortex and the location of the antivortex can be controlled. Indeed, the chirality of the vortex is counterclockwise, as the one of the patterned exchange bias field, and the locations of both the antivortex and the 180° Néel wall shift to the top side of the patterned area.

The strength of the patterned exchange bias field determines both the pinning strength of the vortex core and the stability of the vortex-antivortex pair against annihilation, driven by the vortex-antivortex attraction. These two aspects are studied via micromagnetic simulations, as shown in Fig. 2. In panel (a), the black line and circles show the minimum exchange bias field strength H_{eb} needed for stabilizing the vortex-antivortex pair, as a function of the lateral size of the square pattern L. We observe that, by increasing the size of the patterned area from 0.125 μm to 1 μm, the minimum exchange bias field required decreases from 55 mT down to 2.5 mT. Such a trend reflects the fact that by increasing the pattern size, the distance between the equilibrium positions of the vortex and antivortex increases, which in turn leads to a weaker attractive force that can be countered by weaker exchange bias fields. The red curve and squares show the corresponding distance A between the vortex and the antivortex, ranging from 50 nm to 450 nm. As shown schematically in the inset, the equilibrium positions do not represent the geometrical center, for the vortex, and corner, for the antivortex, due to the attractive force between the vortex and the antivortex. In panel (b), we study via micromagnetic simulations the displacement D of the vortex core from its equilibrium position as a function of small external applied fields, for systems characterized by different exchange bias fields. The simulated pattern size is a 5 μm square, and therefore, the vortex core equilibrium position is located in the geometrical center of the pattern due to the large distance between the vortex and the antivortex. The inset displays the micromagnetic configuration of the system for $H_{eb} = 6\,\text{mT}$ and $H_{ext} = 5\,\text{mT}$, showing the vortex core and the 90° Néel domain wall displacement with respect to the initial

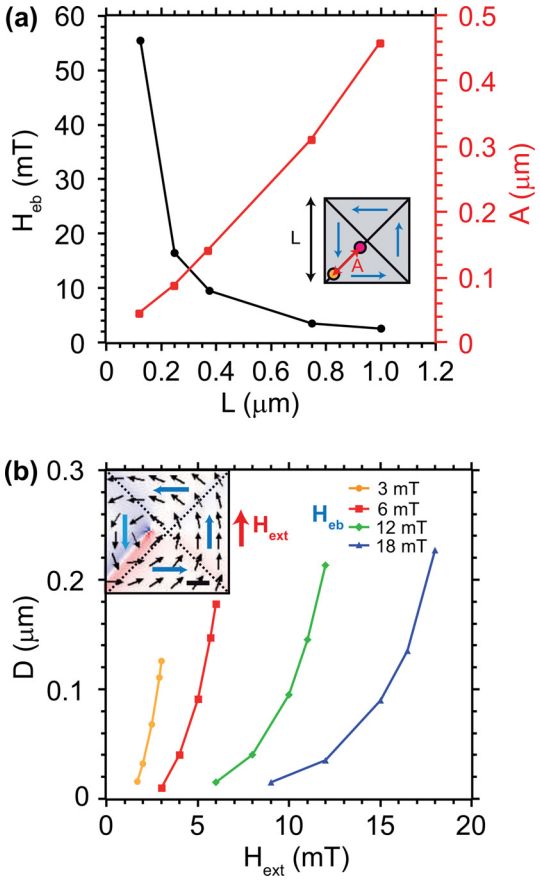

FIG. 2. (a) Results of micromagnetic simulations showing the minimum exchange bias field strength H_{eb} needed for stabilizing vortex-antivortex pairs in the configuration shown in the inset, as a function of the lateral size of the pattern L. The corresponding distance A between the vortex and the antivortex is shown in red. (b) Distance D between the vortex core and the geometrical center of the pattern, as a function of the external magnetic field H_{ext}, for different exchange bias field strengths ranging from 3 mT up to 18 mT. In the inset, micromagnetic simulation showing the vortex core displacement and the orientation of the external magnetic field. The scale bar is 100 nm.

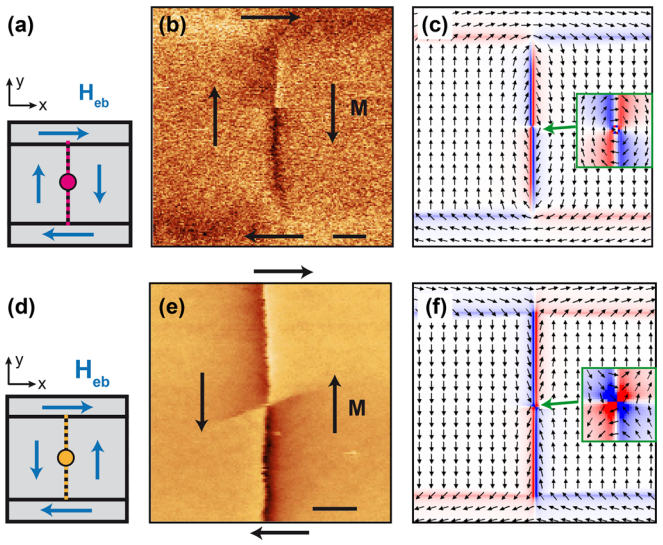

FIG. 3. Stabilization of antivortex and vortex Bloch lines within patterned domain walls. (a) and (d) Sketches showing the geometry and direction of the patterned exchange bias for stabilizing vortex and antivortex Bloch lines, respectively. The vortex (antivortex) Bloch line is indicated by the pink (yellow) circle, and the corresponding 180° Néel domain wall is marked by the dashed line. The direction of the exchange bias field is indicated in blue for each patterned area. (b) and (e) MFM images of the patterned structures for the vortex and antivortex Bloch lines, respectively. The direction of the magnetization is indicated by the black arrows. The opposite bright-dark colors in the top and bottom parts of the domain wall confirm the change in the wall chirality and the stabilization of the Bloch line in both cases. The scale bar is 3 μm. (c) and (f) Simulated micromagnetic configuration for the vortex and antivortex Bloch lines, respectively. The black arrows indicate the direction of the spins, and the red/blue color marks div (**M**), which is related to the MFM contrast.

equilibrium position. As expected, we observe that the core displacement induced by the external field decreases for increasing exchange bias fields ranging from 3 mT up to 18 mT, due to the increased pinning strength associated with the unidirectional anisotropy.

In the following, we demonstrate that it is possible to deterministically stabilize either vortex or antivortex Bloch lines (also named circular and cross Bloch lines, respectively) with tailored chirality within patterned Néel domain walls, by properly designing the boundary conditions at the domain wall edges. Furthermore, we show that the patterned domain wall constitutes a nanoscale racetrack for Bloch lines, which can be controlled and steered along the wall via external fields.

In Figs. 3(a)–3(c), we show experimentally and with simulations the stabilization of a vortex Bloch line within a patterned 180° Néel wall, in a CoFeB 20/IrMn 10/Ru 2 (thicknesses in nm) system. In panel (a), a sketch of the configuration of the patterned exchange bias is shown. The 180° wall is defined by rectangular regions with magnetization oriented in opposite directions along $+y$ and $-y$. In such a system, the orientation of the magnetization within the domain wall, i.e., the chirality of the domain wall, is determined by the boundary conditions and hence by the direction of the magnetization at the edges of the domain wall. The Bloch line is stabilized by imposing two opposite chiralities at the two ends of the wall, by defining two regions with oppositely oriented magnetization. It is worth noting that both the chirality of the Bloch lines and their vorticity, i.e., vortex or antivortex, can be tailored by controlling the orientation of the magnetization of the central domains. In particular, in panel (b), we show the MFM image of a vortex Bloch line with clockwise chirality within a straight 180° Néel wall. The magnetization within the wall points towards $-x$ ($+x$) in the bottom (top) part of the wall, as indicated by the opposite MFM contrast, in good agreement with the micromagnetic simulations of panel (c). The bright/dark colors at the top and bottom sides of the MFM image confirm the opposite direction of the magnetization in the two domains. As shown in panel (e), (f) an antivortex Bloch line is stabilized by patterning an opposite magnetization direction in the two central domains [as sketched in panel (d)].

In Fig. 4, we show, via micromagnetic simulations, that Bloch lines stabilized via tam-SPL can be manipulated within the nanopatterned domain walls via static external magnetic fields, without altering the magnetic configuration of the domain wall at remanence. In order to study the Bloch line motion, a damping parameter $\alpha = 0.02$ was used for these simulations.[39] In panel (a), an antivortex Bloch line is stabilized at the top edge of a straight 180° wall (see sketch on the left), by applying an initialization field H_{init} along $-x$.

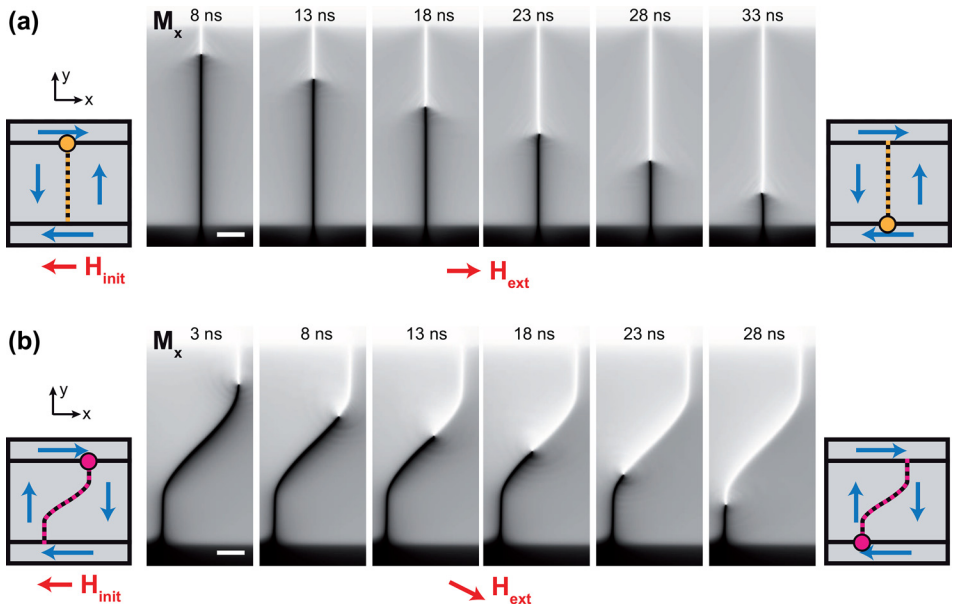

FIG. 4. Manipulation of Bloch lines within nanopatterned 180° walls, via external fields. (a) Controlled displacement as a function of time of an antivortex Bloch line, initially stabilized at the top edge of a straight 180° Néel wall (see sketch on the left), via a 6.7 mT static magnetic field applied along $+x$. (b) Displacement as a function of time of a vortex Bloch line along a zig-zag shaped 180° Néel wall, via a 6.7 mT static external field applied as sketched. The scale bar is 500 nm.

The exchange bias field strength is 12 mT. The central panels show the x-component of the magnetization, which allows us to clearly locate the Bloch line within the wall, as a function of time. From left to right, we show that, by applying a 6.7 mT static external field along $+x$, the Bloch line can be displaced from the top edge down to the bottom edge of the wall (see also supplementary material note 3). During the displacement, the Bloch line passes through metastable states, as shown in supplementary material note 2 and Fig. S2. In panel (b), a vortex Bloch line is stabilized on the top edge of a zig-zag 180° wall. The shape of the wall is determined by the geometry of the patterned central domains, as shown in the sketch on the left. The Bloch line is displaced from its initial position, and interestingly, it follows the complex profile of the wall and stabilizes in proximity of the lower domain, demonstrating the possibility of continuously manipulating Bloch lines along arbitrarily shaped tracks. Crucially for applications, the position and shape of the domain wall at remanence, which are determined by the patterned exchange bias profile, are not affected by the field applied for the Bloch line displacement (see supplementary material note 2 and Fig. S2).

In conclusion, we presented a strategy for the reversible, non-volatile stabilization and nanoscale manipulation of magnetic vortices and Bloch lines, within continuous exchange bias systems. We showed that, by vectorially nanopatterning the unidirectional magnetic anisotropy, it is possible to stabilize vortices with the controlled position, vorticity, and chirality and to deterministically stabilize cross and circular Bloch lines within patterned arbitrarily shaped Néel domain walls. Finally, we showed that such domain walls can be employed as reconfigurable conduits where the Bloch lines are manipulated and displaced via static external fields. Our work opens the way towards the study and integration of functionalities based on tailored topological spin-textures in next-generation spintronic and spin-wave devices, such as finely tuned spin-wave emitters/detectors and magnetic oscillators based on arrays of coupled vortices.

See supplementary material for details on the high-temperature cantilever design and for the results of additional micromagnetic simulations on the propagation of Bloch lines along nanopatterned domain walls.

The authors thank Professor Riccardo Bertacco and Professor Hans Hug for the valuable discussions. The research leading to these results received funding from the European Union's Horizon 2020 research and innovation programme under Grant Agreement No. 705326, project SWING. We acknowledge the support from the Office of Basic Energy Sciences of the U.S. Department of Energy (Grant No. DE-SC0016204) and the U.S. Army Research Office and the U.S. National Science Foundation (NSF). This work was partially performed at Polifab, the micro- and nano-technology center of the Politecnico di Milano.

[1]T. H. Kim, S. Cheon, and H. W. Yeom, Nat. Phys. **13**, 444 (2017).
[2]G. Finocchio, F. Büttner, R. Tomasello, M. Carpentieri, and M. Kläui, J. Phys. D: Appl. Phys. **49**, 423001 (2016).
[3]G. Hrkac, P. S. Keatley, M. T. Bryan, and K. Butler, J. Phys. D: Appl. Phys. **48**, 453001 (2015).
[4]S. Zhang, A. A. Baker, S. Komineas, and T. Hesjedal, Sci. Rep. **5**, 15773 (2015).
[5]D. Kumar, S. Barman, and A. Barman, Sci. Rep. **4**, 4108 (2015).
[6]D.-H. Kim, E. A. Rozhkova, I. V. Ulasov, S. D. Bader, T. Rajh, M. S. Lesniak, and V. Novosad, Nat. Mater. **9**, 165 (2010).
[7]S. S. P. Parkin, M. Hayashi, and L. Thomas, Science **320**, 190 (2008).
[8]A. Fert, V. Cros, and J. Sampaio, Nat. Nanotechnol. **8**, 152 (2013).
[9]L. D. Geng and Y. M. Jin, J. Magn. Magn. Mater. **423**, 84 (2017).
[10]S. Kaka, M. R. Pufall, W. H. Rippard, T. J. Silva, S. E. Russek, and J. A. Katine, Nature **437**, 389 (2005).
[11]B. Van Waeyenberge, A. Puzic, H. Stoll, K. W. Chou, T. Tyliszczak, R. Hertel, M. Fähnle, H. Brückl, K. Rott, G. Reiss, I. Neudecker, D. Weiss, C. H. Back, and G. Schütz, Nature **444**, 461 (2006).
[12]K. Yamada, S. Kasai, Y. Nakatani, K. Kobayashi, H. Kohno, A. Thiaville, and T. Ono, Nat. Mater. **6**, 270 (2007).
[13]M. Manfrini, J. Von Kim, S. Petit-Watelot, W. Van Roy, L. Lagae, C. Chappert, and T. Devolder, Nat. Nanotechnol. **9**, 121 (2014).
[14]S. B. Choe, Y. Acremann, A. Scholl, A. Bauer, A. Doran, J. Stöhr, and H. A. Padmore, Science **304**, 420 (2004).
[15]V. S. Pribiag, I. N. Krivorotov, G. D. Fuchs, P. M. Braganca, O. Ozatay, J. C. Sankey, D. C. Ralph, and R. A. Buhrman, Nat. Phys. **3**, 498 (2007).
[16]Q. Mistral, M. van Kampen, G. Hrkac, J.-V. Kim, T. Devolder, P. Crozat, C. Chappert, L. Lagae, and T. Schrefl, Phys. Rev. Lett. **100**, 257201 (2008).

[17]A. Ruotolo, V. Cros, B. Georges, A. Dussaux, J. Grollier, C. Deranlot, R. Guillemet, K. Bouzehouane, S. Fusil, and A. Fert, Nat. Nanotechnol. **4**, 528 (2009).
[18]Y. Yoshimura, K.-J. Kim, T. Taniguchi, T. Tono, K. Ueda, R. Hiramatsu, T. Moriyama, K. Yamada, Y. Nakatani, and T. Ono, Nat. Phys. **12**, 157 (2016).
[19]S. Emori, U. Bauer, S.-M. Ahn, E. Martinez, and G. S. D. Beach, Nat. Mater. **12**, 611 (2013).
[20]J. P. Park and P. A. Crowell, Phys. Rev. Lett. **95**, 167201 (2005).
[21]M. Kammerer, M. Weigand, M. Curcic, M. Noske, M. Sproll, A. Vansteenkiste, B. Van Waeyenberge, H. Stoll, G. Woltersdorf, C. H. Back, and G. Schuetz, Nat. Commun. **2**, 279 (2011).
[22]M.-W. Yoo, J. Lee, and S.-K. Kim, Appl. Phys. Lett. **100**, 172413 (2012).
[23]S. Wintz, V. Tiberkevich, M. Weigand, J. Raabe, J. Lindner, A. Erbe, A. Slavin, and J. Fassbender, Nat. Nanotechnol. **11**, 948 (2016).
[24]T. Shinjo, T. Okuno, R. Hassdorf, K. Shigeto, and T. Ono, Science **289**, 930 (2000).
[25]K. S. Buchanan, P. E. Roy, M. Grimsditch, F. Y. Fradin, K. Y. Guslienko, S. D. Bader, and V. Novosad, Nat. Phys. **1**, 172 (2005).
[26]T. Devolder, J. Von Kim, M. Manfrini, W. Van Roy, L. Lagae, and C. Chappert, Appl. Phys. Lett. **97**, 072512 (2010).
[27]J. Li, A. Tan, K. W. Moon, A. Doran, M. A. Marcus, A. T. Young, E. Arenholz, S. Ma, R. F. Yang, C. Hwang, and Z. Q. Qiu, Appl. Phys. Lett. **104**, 262409 (2014).
[28]Y. Gaididei, O. M. Volkov, V. P. Kravchuk, and D. D. Sheka, Phys. Rev. B **86**, 144401 (2012).
[29]K. Kuepper, M. Buess, J. Raabe, C. Quitmann, and J. Fassbender, Phys. Rev. Lett. **99**, 167202 (2007).
[30]E. Albisetti, D. Petti, M. Pancaldi, M. Madami, S. Tacchi, J. Curtis, W. P. King, A. Papp, G. Csaba, W. Porod, P. Vavassori, E. Riedo, and R. Bertacco, Nat. Nanotechnol. **11**, 545 (2016).
[31]E. Albisetti, D. Petti, M. Madami, S. Tacchi, P. Vavassori, E. Riedo, and R. Bertacco, AIP Adv. **7**, 055601 (2017).
[32]E. Albisetti, D. Petti, G. Sala, R. Silvani, S. Tacchi, S. Finizio, S. Wintz, A. Caló, X. Zheng, J. Raabe, E. Riedo, and R. Bertacco, Commun. Phys. **1**, 56 (2018).
[33]E. Albisetti and D. Petti, J. Magn. Magn. Mater. **400**, 230 (2016).
[34]M. Spieser, C. Rawlings, E. Lörtscher, U. Duerig, and A. W. Knoll, J. Appl. Phys. **121**, 174503 (2017).
[35]A. Vansteenkiste, J. Leliaert, M. Dvornik, M. Helsen, F. Garcia-Sanchez, and B. Van Waeyenberge, AIP Adv. **4**, 107133 (2014).
[36]D. Petti, E. Albisetti, H. Reichlová, J. Gazquez, M. Varela, M. Molina-Ruiz, A. F. Lopeandía, K. Olejník, V. Novák, I. Fina, B. Dkhil, J. Hayakawa, X. Marti, J. Wunderlich, T. Jungwirth, and R. Bertacco, Appl. Phys. Lett. **102**, 192404 (2013).
[37]P. P. Sharma, E. Albisetti, M. Massetti, M. Scolari, C. La Torre, M. Monticelli, M. Leone, F. Damin, G. Gervasoni, G. Ferrari, F. Salice, E. Cerquaglia, G. Falduti, M. Cretich, E. Marchisio, M. Chiari, M. Sampietro, D. Petti, and R. Bertacco, Sens. Actuators, B **242**, 280 (2017).
[38]D. Holzinger, N. Zingsem, I. Koch, A. Gaul, M. Fohler, C. Schmidt, and A. Ehresmann, J. Appl. Phys. **114**, 13908 (2013).
[39]M. C. Weber, H. Nembach, B. Hillebrands, M. J. Carey, and J. Fassbender, J. Appl. Phys. **99**, 08J308 (2006).